Full Paper

CSIRO PUBLISHING

Aust. J. Chem. **2005**, *58*, 472–482

www.publish.csiro.au/journals/ajc

Helical Porous Protein Mimics Self-Assembled from Amphiphilic Dendritic Dipeptides*

Virgil Percec,[A,C] *Andrés Dulcey*,[A] *Mihai Peterca*,[B] *Monica Ilies*,[A] *Yoshiko Miura*,[A] *Ulrica Edlund*,[A] *and Paul A. Heiney*[B]

[A] Roy & Diana Vagelos Laboratories, Department of Chemistry, Laboratory for Research on the Structure of Matter, University of Pennsylvania, Philadelphia, PA 19104-6323, USA.

[B] Department of Physics and Astronomy, Laboratory for Research on the Structure of Matter, University of Pennsylvania, Philadelphia, PA 19104-6396, USA.

[C] Corresponding author. Email: percec@sas.upenn.edu

This manuscript reports the synthesis and the self-assembly of (4-3,4,5-3,5)nG$_2$-CH$_2$-Boc-L-Tyr-L-Ala-OMe dendritic dipeptides ($n = 12$, 16). These dendritic dipeptides self-assemble both in solution and in solid states into helical porous supramolecular columns that mimic porous transmembrane proteins. These supramolecular assemblies provide also a new class of tubular supramolecular polymers.

Manuscript received: 21 April 2005.
Final version: 1 May 2005.

Introduction

A recent communication from our laboratory reported a new class of amphiphilic dendritic dipeptides that self-assemble both in solution and in bulk into supramolecular helical porous or tubular structures.[1] This class of self-assembling building blocks provides a general synthetic strategy to mimic the structure of porous transmembrane proteins. Porous transmembrane proteins and their remodelled structures perform a multitude of biological functions such as viral helical coats,[2] transmembrane channels,[3,4] mediated protein folding,[5] reversible encapsulation,[6] stochastic sensing,[7] and pathogenic[8] or antibacterial[9] activity. In that previous communication[1] we reported the synthesis, the mechanism of self-assembly, and the structural analysis of the supramolecular porous structures generated from the dendritic dipeptides (4-3,4-3,5)12G$_2$-CH$_2$-Boc-L-Tyr-L-Ala-OMe and (4-3,4-3,5)12G$_2$-CH$_2$-Boc-D-Tyr-D-Ala-OMe (Scheme 1). We also presented preliminary data showing that a diversity of other dendritic dipeptides constructed from the same amphiphilic (4-3,4-3,5)12G$_2$-CH$_2$- dendron attached to other dipeptides, as well as other amphiphilic dendrons attached to the same Boc-L-Tyr-L-Ala-OMe dipeptide, self-assemble into porous supramolecular structures. These porous protein mimics also represent a new class of supramolecular tubular polymers with three-dimensional structure controlled in a cooperative way by the stereochemistry of the dipeptide and by the primary structure of the amphiphilic dendron.[1]

In this paper we report the synthesis (Schemes 2–4), the structural analysis, and the self-assembly of the amphiphilic dendritic dipeptides (4-3,4,5-3,5)nG$_2$-CH$_2$-Boc-L-Tyr-L-Ala-OMe ($n = 12$, 16) and discuss the similarities and differences between their supramolecular structures and the structures generated from (4-3,4-3,5)12G$_2$-CH$_2$-Boc-L-Tyr-L-Ala-OMe dendritic dipeptide (Scheme 1).

Results and Discussion

The synthesis of (4-3,4,5-3,5)nG$_2$-CH$_2$-Boc-L-Tyr-L-Ala-OMe follows the sequence of reactions summarized in Schemes 2–4. The precursors (4-3,4,5)12G$_2$-CH$_2$Cl and (4-3,4,5)16G$_2$-CH$_2$Cl were synthesized as illustrated in Scheme 2.[10] The structure of both dendritic dipeptides was confirmed by a combination of 500-MHz ^{1}H and 125-MHz ^{13}C NMR spectroscopy and their purity was shown to be higher than 99% by a combination of thin layer chromatography (TLC), high pressure liquid chromatography (HPLC), and matrix-assisted laser desorption–ionization time-of-flight (MALDI-TOF) mass spectrometry.

During the self-assembly process the dendron mimics, through its monodisperse primary structure, the most fundamental structural principles of a protein. The conformational freedom of the benzyl ether units resembles the conformational freedom of the peptide bond. The 4-3,4,5-3,5 distribution of repeat units sequences and the amphiphilic character introduced by the alkyl tails of the dendron resemble the precise primary structure and the hydrophobic sequences of

* Part of this research was discussed in a plenary lecture presented by V.P. at the 27th Australasian Polymer Symposium, 28 November–2 December 2004, Adelaide.

10.1071/CH05092 0004-9425/05/060472

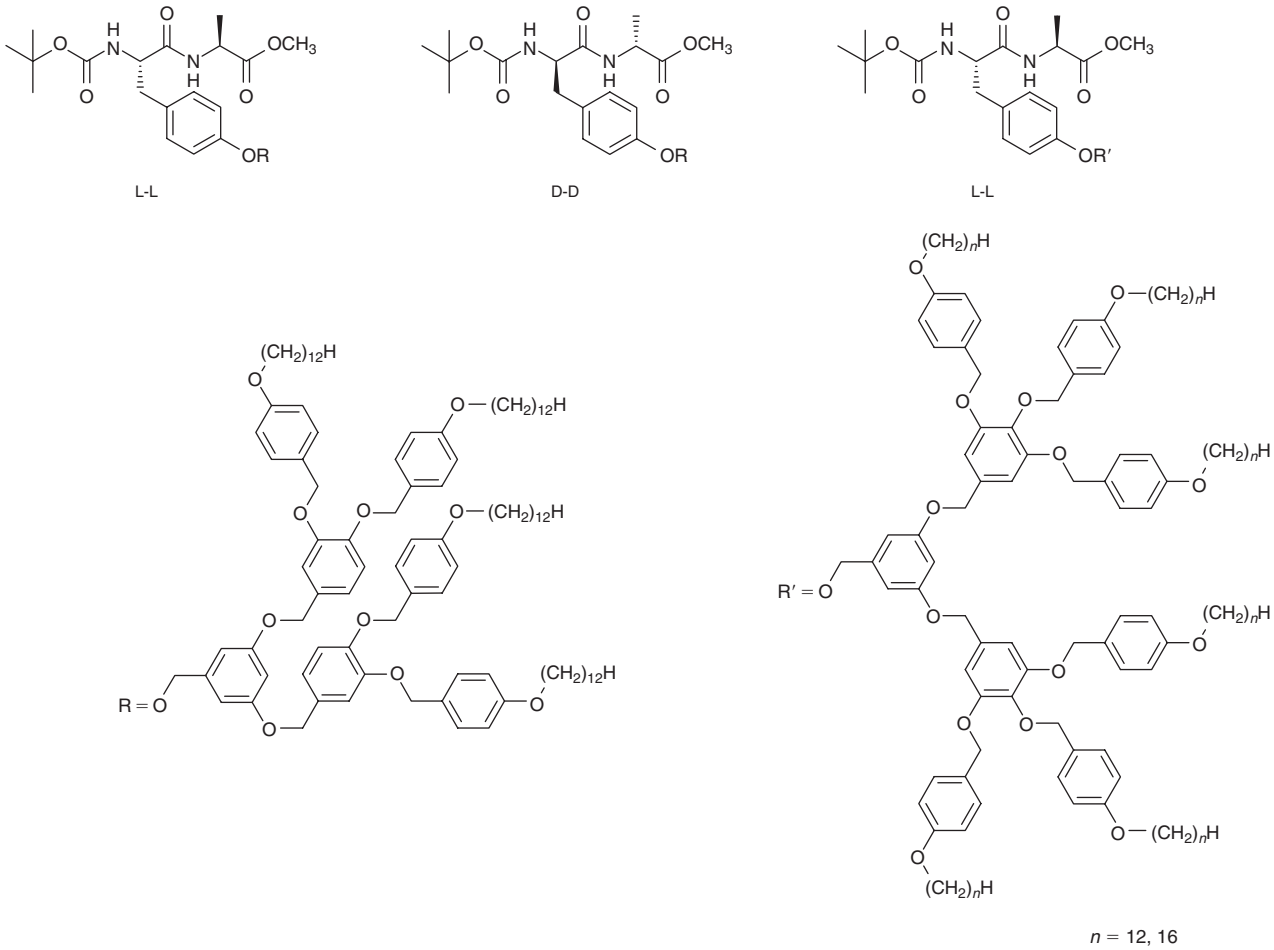

Scheme 1. L-L and D-D stereoisomers of (4-3,4-3,5)12G_2-CH_2-Boc-Tyr-Ala-OMe and (4-3,4,5-3,5)*n*G_2-CH_2-Boc-L-Tyr-L-Ala-OMe ($n = 12, 16$).

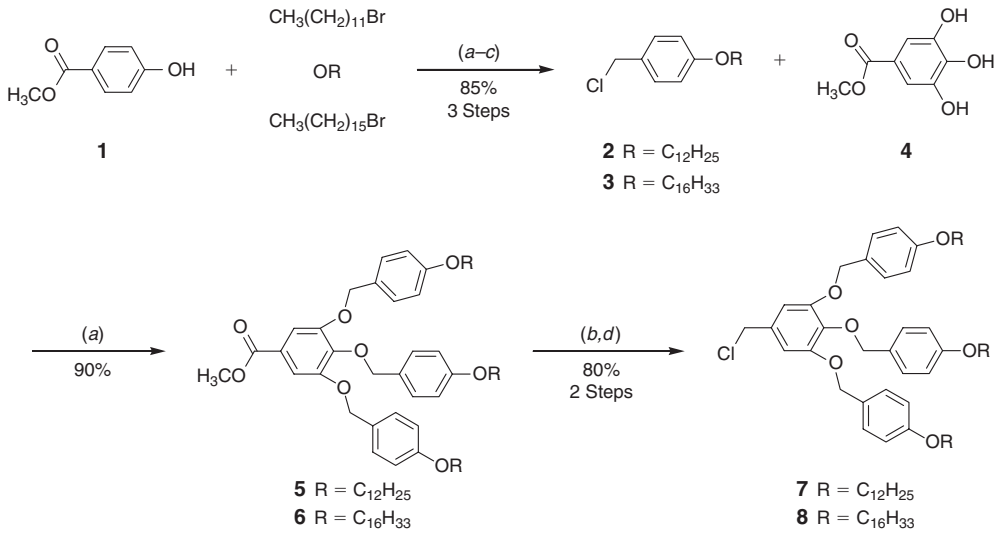

Scheme 2. Synthesis of (4-3,4,5-3,5)*n*G_1-CH_2Cl ($n = 12, 16$). Reagents and conditions: (*a*) K_2CO_3, DMF, 70°C; (*b*) LAH, THF; (*c*) $SOCl_2$, CH_2Cl_2, cat. DMF; (*d*) $SOCl_2$, DTBMP, CH_2Cl_2.

proteins. The Boc-L-Tyr-L-Ala-OMe dipeptide fragment of the dendritic dipeptide plays the role of a tag that detects structural informations of the dendron in dilute solution and in the solid state. For example, the ability of the dipeptide to form hydrogen bonds in solution indicates an *all-trans* benzyl ether conformation that generates the tapered shape of the dendron. This tapered shape facilitates the self-assembly process. The inability of the dipeptide to form hydrogen bonds

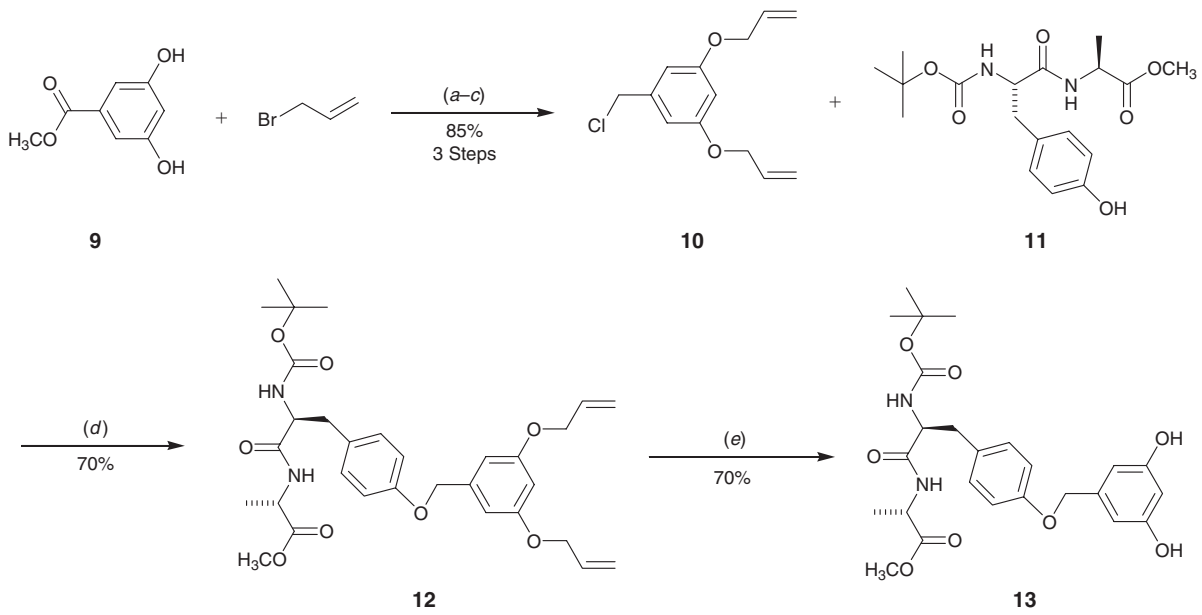

Scheme 3. Synthesis of the dendritic dipeptide precursor [3,5]OHG$_1$-CH$_2$-Boc-L-Tyr-L-Ala-OMe. Reagents and conditions: (*a*) K_2CO_3, acetone, reflux; (*b*) LAH, THF; (*c*) $SOCl_2$, CH_2Cl_2, cat. DMF; (*d*) K_2CO_3, DMF, 70°C; (*e*) $Pd(OAc)_2$, PPh_3, Et_3NHCO_2H, EtOH, reflux.

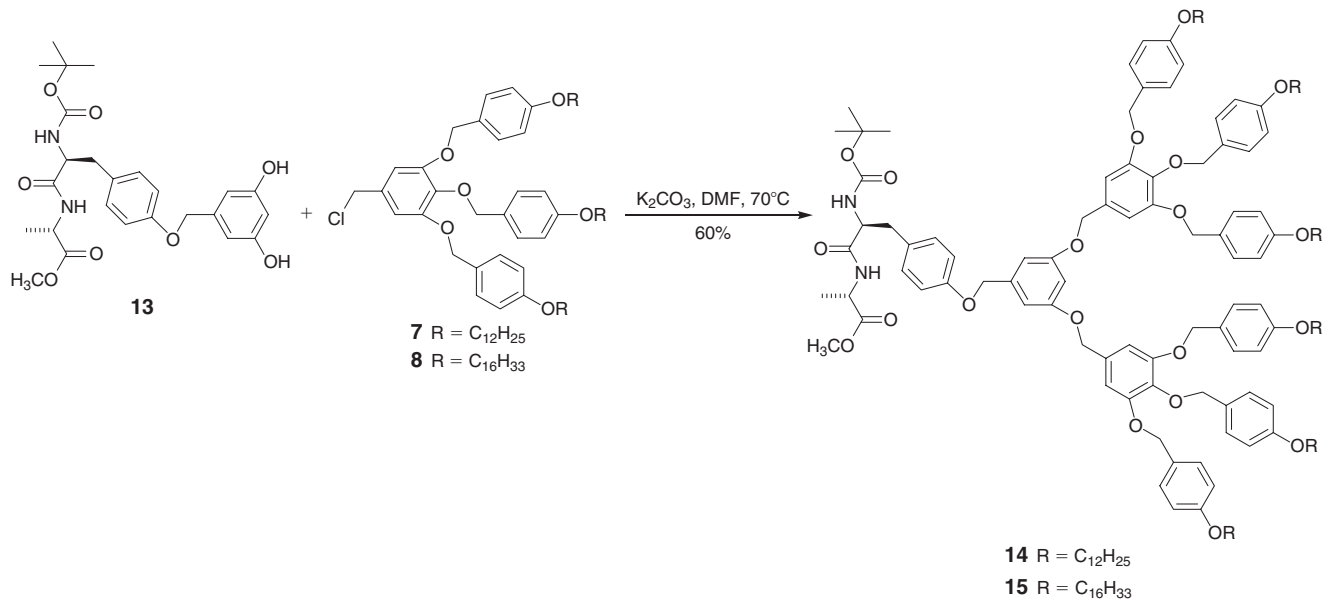

Scheme 4. Synthesis of (4-3,4,5-3,5)*n*G$_2$-CH$_2$-Boc-L-Tyr-L-Ala-OMe and (4-3,4,5-3,5)*n*G$_2$-CH$_2$-Boc-D-Tyr-D-Ala-OMe ($n = 12, 16$).

in a good solvent for hydrogen bonding, such as chloroform or methylene chloride, arises from the dynamic equilibrium between the *trans* and *gauche* conformers of the dendron. This dynamic equilibrium induces a globular conformation of the dendron (Scheme 5).

For steric reasons the globular dendron conformation contains the dipeptide at the focal point and, therefore, prohibits self-assembly in solution. By using this strategy, ^{1}H NMR spectroscopy was used to select solvophobic solvents for the dendritic dipeptide.[1] Solvophobic solvents change the dynamic equilibrium between *trans* and *gauche* conformers of the benzyl ether into an *all-trans* conformation (Scheme 5). This process is similar to the hydrophobic effect provided by water during the folding of proteins. The second role of the dipeptide tag is to detect the helical structure of the supramolecular assembly in solution.

By using a combination of 500-MHz ^{1}H NMR spectroscopy, UV spectroscopy, and circular dichroism (CD) we found that (4-3,4,5-3,5)12G$_2$-CH$_2$-Boc-L-Tyr-L-Ala-OMe adopts an *all-trans* conformation in the solvophobic solvents cyclohexane and hexane. Figs 1 and 2 show the UV and CD spectra of (4-3,4,5-3,5)12G$_2$-CH$_2$-Boc-L-Tyr-L-Ala-OMe and of (4-3,4,5-3,5)16G$_2$-CH$_2$-Boc-L-Tyr-L-Ala-OMe, respectively, in cyclohexane as a function of temperature.

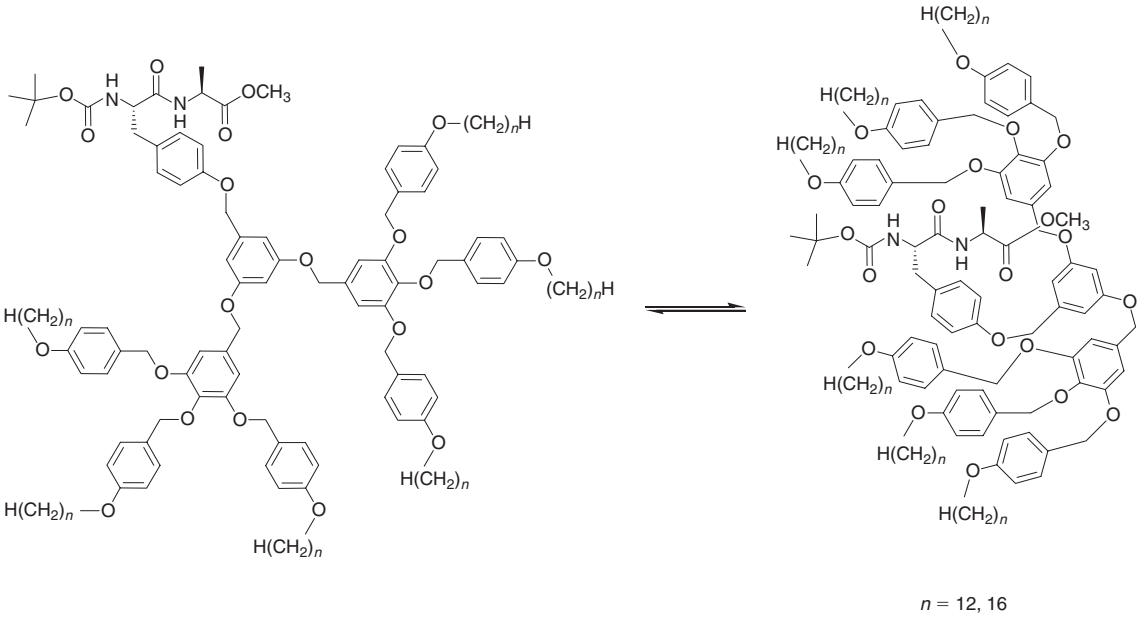

Scheme 5. *Trans*-tapered low-temperature (left) and globular high-temperature (right) conformers of (4-3,4,5-3,5)*n*G_2-CH_2-Boc-L-Tyr-L- Ala-OMe ($n = 12$, 16).

In both cases increasing the temperature from below 10 to 32°C generates an increase of UV absorption at 230 nm. This indicates a change in dendron conformation from globular to tapered. From 34 to 60°C this absorption decreases sharply and subsequently remains constant (Figs 1*a* and 2*a*). This shows an intermolecular self-assembly process. ^{1}H NMR analysis of this process demonstrates that, during the self-assembly process, hydrogen bonding takes place.[1] In the CD spectra of both compounds (Figs 1*b* and 2*b*) from 34 to 60°C, only the Cotton effect associated with the ellipticity of the dendritic dipeptide at 230 nm is observed. Below 34°C the CD spectra correspond to the aromatic part of the dendron, and indicate a helical structure in the supramolecular dendron whose helix sense is selected by the stereochemistry of the dipeptide.

The detailed structural analysis of the supramolecular structure resulted from (4-3,4,5-3,5)*n*G_2-CH_2-Boc-L-Tyr-L-Ala-OMe ($n = 12$, 16) was carried out by small-angle X-ray diffraction (XRD) on powder and by a combination of small and wide-angle XRD on oriented fibres, after phase-transition temperatures were determined by differential scanning calorimetry (DSC) experiments. The DSC analysis (Fig. 3) shows that in bulk state both dendritic dipeptides self-assemble into supramolecular columns that self-organize in two-dimensional column hexagonal (Φ_h) lattices. These lattices facilitate the analysis of the supramolecular columns by XRD experiments. Both dendritic dipeptides present, after their glass transition, a three-dimensional columnar hexagonal lattice with long-range order. This three-dimensional order is not observed in the case of the lattice generated from the (4-3,4-3,5)12G_2-CH_2-Boc-L-Tyr-L-Ala-OMe dendritic dipeptides. The higher order of this three-dimensional lattice is in agreement with the increase in the intensity of the Cotton effect observed for (4-3,4,5-3,5)*n*G_2-CH_2-Boc-L-Tyr-L-Ala-OMe ($n = 12$, 16) in Figs 1*b* and 2*b*, respectively, as compared to the (4-3,4-3,5)12G_2-CH_2-Boc-L-Tyr-L-Ala-OMe.[1]

Both dendritic dipeptides exhibit a complex set of columnar hexagonal lattices that are strongly dependent on temperature. The small-angle XRD powder diffractograms are presented in Fig. 4 while small- and wide-angle patterns obtained from an oriented fibre are shown in Fig. 5.

The enhanced integrated intensity of the (11), (20), and (21) reflections from Fig. 4 indicate a porous column. However, the intensities of these reflections are not as strong as those of the supramolecular structures generated from (4-3,4-3,5)12G_2-CH_2-Boc-Tyr-Ala-OMe with L-L, D-D, L-D, D-L, and DL-DL stereochemistries. This indicates a smaller pore diameter for the (4-3,4,5-3,5)16G_2-CH_2-Boc-L-Tyr-L-Ala-OMe- and (4-3,4,5-3,5)12G_2-CH_2-Boc-L-Tyr-L-Ala-OMe-derived columns than for the (4-3,4-3,5)12G_2-CH_2-Boc-Tyr-Ala-OMe columns with L-L, D-D, L-D, D-L, and DL-DL stereochemistries. The column and pore diameters (D_{col}, D_{pore}) computed by methods elaborated previously[1] are reported in Table 1.

The XRD data from Fig. 5 support the helical structure detected by CD experiments (Figs 1 and 2) and provide additional details such as dendron tilt angle and registry along the column axis. The three-dimensional structure of the porous assemblies of (4-3,4,5-3,5)16G_2-CH_2-Boc-L-Tyr-L-Ala-OMe calculated from these XRD experiments is shown in Fig. 6.

The pore structure is hydrophobic (Fig. 6*b*). It contains only the methyl groups of Ala (white) and a methyl group from Boc (blue). The hydrophobic part of the dipeptide is incorporated between the hydrophobic part of the pore and

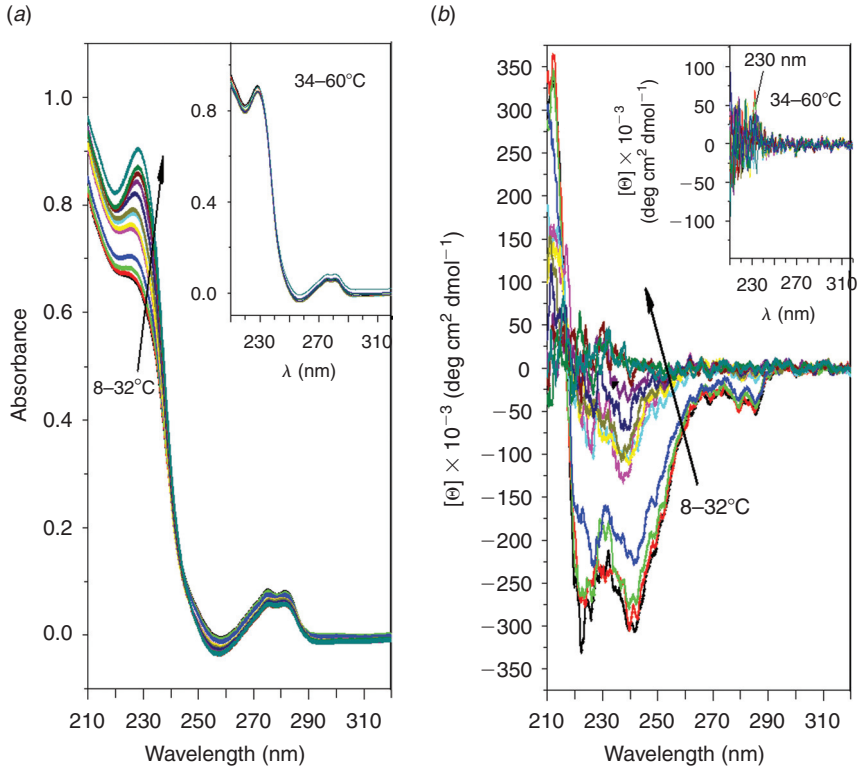

Fig. 1. Spectroscopic analysis of the self-assembly of the dendritic dipeptide (4-3,4,5-3,5)12G_2-CH_2-Boc-L-Tyr-L-Ala-OMe in cyclohexane (0.5×10^{-4} M). (*a*) UV spectra; (*b*) CD spectra. Arrows indicate trends upon increasing temperature from 8 to 32°C. Insets: (*a*) UV absorption and (*b*) the Cotton effect, respectively, associated with the molecular solution of the dendritic dipeptide.

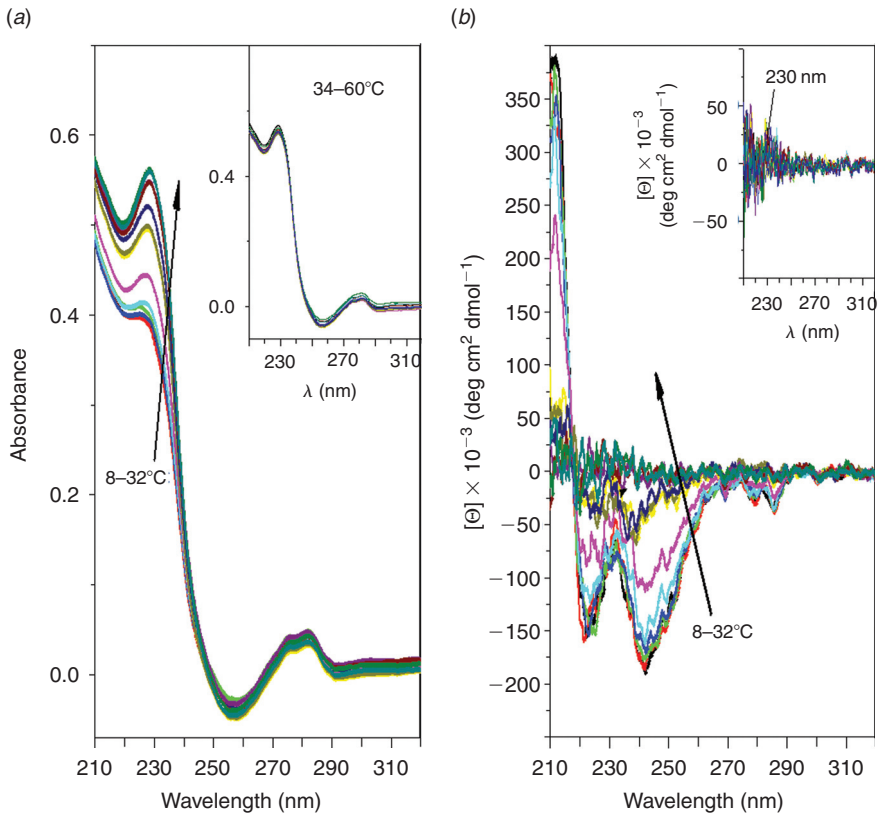

Fig. 2. Spectroscopic analysis of the self-assembly of the dendritic dipeptide (4-3,4,5-3,5)16G_2-CH_2-Boc-L-Tyr-L-Ala-OMe in cyclohexane (0.5×10^{-4} M). (*a*) UV spectra; (*b*) CD spectra. Arrows indicate trends upon increasing temperature from 8 to 32°C. Insets: (*a*) UV absorption and (*b*) the Cotton effect, respectively, associated with the molecular solution of the dendritic dipeptide.

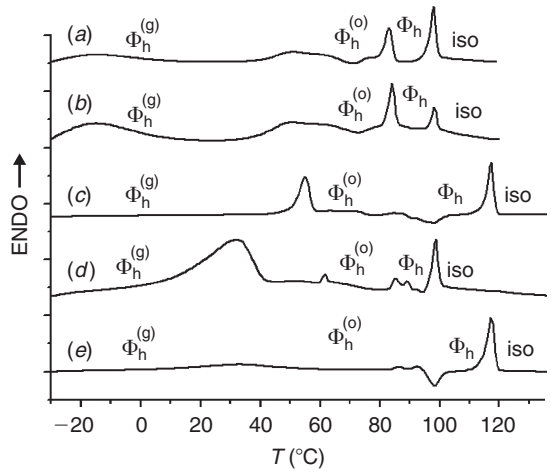

Fig. 3. DSC traces for the assemblies generated from (4-3,4,5-3,5) nG$_2$-CH$_2$-Boc-L-Tyr-L-Ala-OMe with $n = 12$ for (*a*) first heating and (*b*) second heating, and with $n = 16$ for (*c*) first heating and (*d*) second heating and (*e*) third heating after a 30-min annealing at 78°C. Legend: Φ_h: two-dimensional columnar hexagonal lattice; $\Phi_h^{(o)}$: three-dimensional columnar hexagonal lattice; $\Phi_h^{(g)}$: glassy columnar hexagonal lattice.

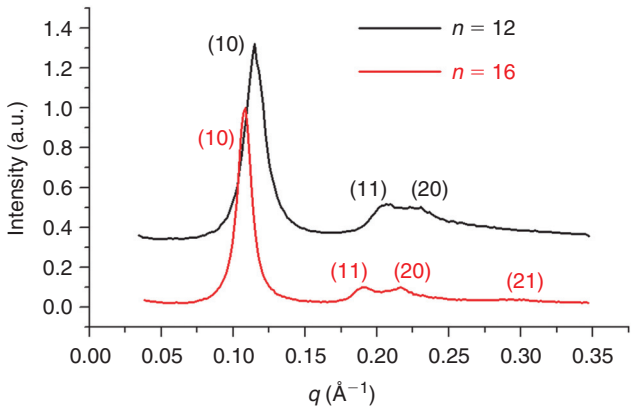

Fig. 4. X-ray diffraction plots for (4-3,4,5-3,5) nG$_2$-CH$_2$-Boc-L-Tyr-L- Ala-OMe ($n = 12$, 16) recorded at 95 and 98°C in their two-dimesional Φ_h lattice.

the hydrophobic dendron. The conformation of the (4-3,4,5-3,5)16G$_2$-CH$_2$-Boc-L-Tyr-L-Ala-OMe in the supramolecular structure from Fig. 6 is shown in Fig. 7*a* and compared with the structure of (4-3,4-3,5)12G$_2$-CH$_2$-Boc-L-Tyr-L-Ala-OMe (Fig. 7*b*).

The difference between the size of the two dendrons observed from their top view projections explains the mechanism responsible for a reduced pore size in the case of the supramolecular column generated from (4-3,4,5-3,5) 16G$_2$-CH$_2$-Boc-L-Tyr-L-Ala-OMe. The wider (4-3,4,5-3,5)nG$_2$-CH$_2$- dendron ($n = 12$, 16) reduces the number of dipeptides that is available to construct the pore in the case of (4-3,4-3,5)12G$_2$-CH$_2$- dendron. This mechanism can be visualized when the top views of the supramolecular pores self-assembled from these two structures are

Table 1. XRD structural analysis of the supramolecular porous columns

(4-3,4,5-3,5)nG$_2$-CH$_2$-Boc-L-Tyr-L-Ala-OMe	$n = 12$	$n = 16$
T [°C]	95	98
Phase	*p6mm*	*p6mm*
d_{10} [Å]^A (I_{10} [a.u.])^B	54.4 (54.12)	57.9 (57.73)
d_{11} [Å]^A (I_{11} [a.u.])^B	30.7 (16.04)	32.7 (14.95)
d_{20} [Å]^A (I_{20} [a.u.])^B	27.9 (29.84)	29.2 (15.57)
d_{21} [Å]^A (I_{21} [a.u.])^B		21.0 (11.74)
$a = D_{col}$ [Å]	62.9 ± 0.4	66.6 ± 0.4
D_{pore} [Å]	9.2 ± 1.5	8.7 ± 1.3

^{A} *d*-spacings of columnar hexagonal phase.
^{B} Peak integrated intensity scaled to the sum of the observed diffraction peaks.

compared (Fig. 8). The (4-3,4,5-3,5)nG$_2$-CH$_2$-Boc-L-Tyr-L-Ala-OMe ($n = 12$, 16) supramolecular columns show a decrease of the column diameter of more than 10 Å as compared to (4-3,4-3,5)12G$_2$-CH$_2$-Boc-L-Tyr-L-Ala-OMe (data compared at the same temperature), whereas the observed dendron tilt and stacking distance along the column is almost unchanged. Consequently, the number of dendritic dipeptide units forming a layer is six for (4-3,4,5-3,5)nG$_2$-CH$_2$-Boc-L-Tyr-L-Ala-OMe ($n = 12$, 16) and twelve for (4-3,4-3,5)12G$_2$-CH$_2$-Boc-L-Tyr-L-Ala-OMe. This difference dictates a different structure of the hydrogen-bonding network (Fig. 9).

In contrast to the (4-3,4-3,5)12G$_2$-CH$_2$-Boc-L-Tyr-L-Ala-OMe structure, the in-layer hydrogen bonds do not form due to the increased separation between the in-layer adjacent dipeptides. The increase in separation is caused by the smaller number of dendritic dipeptides units per layer. The structure of the hydrogen bond network of (4-3,4,5-3,5)nG$_2$-CH$_2$-Boc-L-Tyr-L-Ala-OMe ($n = 12$, 16) is formed between the ith and ($i \pm 7$)th units (that is, cross-layer only).The hierarchical mechanism of pore assembly can be envisioned by the sequence of pore structures presented in Fig. 9.

Conclusions

This publication reports the second example of dendritic dipeptide that self-assembles in supramolecular porous structures. The structures, together with the one reported previously,[1] provide a new class of supramolecular polymers. The change in the structure of the dendritic dipeptide from (4-3,4-3,5)12G$_2$-CH$_2$-Boc-L-Tyr-L-Ala-OMe to (4-3,4,5-3,5)12G$_2$-CH$_2$-Boc-L-Tyr-L-Ala-OMe mediates a reduction of the pore diameter. These experiments provide the first example of pore size design by using a single dipeptide and different dendrons in the structure of the dendritic dipeptide. These results open numerous synthetic strategies for the design of supramolecular tubular polymers. The self-assembled structures reported in this publication are complementary to concepts elaborated in other laboratories.[11–13] This class of porous assemblies provides one of the few examples of synthetic supramolecular architectures that

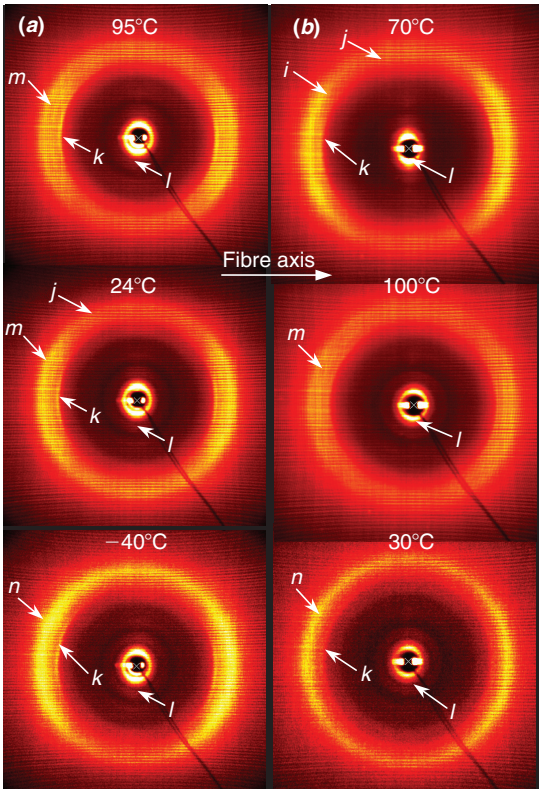

Fig. 5. X-ray diffraction patterns of aligned fibre samples: (*a*) (4-3,4,5-3,5)12G$_2$-CH$_2$-Boc-L-Tyr-L-Ala-OMe and (*b*) (4-3,4,5-3,5)16G$_2$-CH$_2$-Boc-L-Tyr-L-Ala-OMe. Legend: *i*: short-range helical feature (~4.5 ± 0.2 Å); *j*: tilt (~62 ± 5°); *k*: registry along the column axis (~5 ± 0.2 Å); *l*: (*hk*0) reflections of the *p6mm* columnar phase; *m*: (*hkl*) crystal reflections; *n*: reflection of the aliphatic tails in the glassy phase. The temperature at which the XRD scans were recorded is indicated on each diffraction pattern.

exhibit tertiary and quaternary structures.[13] These tubular supramolecular polymers complement other supramolecular concepts reported previously from our[14–18] and other laboratories.[19,20]

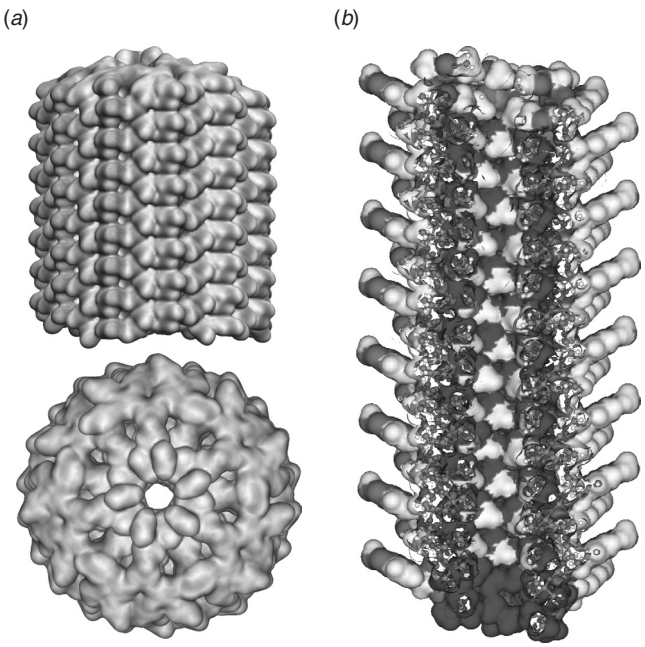

Fig. 6. The structure of the supramolecular porous column self-assembled from (4-3,4,5-3,5)16G$_2$-CH$_2$-Boc-L-Tyr-L-Ala-OMe. (*a*) Side and top Van der Waals surface views of the supramolecular column; for simplicity the aliphatic tails are not shown. (*b*) Cross-section through the hydrophobic pore; the dendrons are shown up to the phenyl groups of Tyr. Legend: Boc: blue; NH: green; O: red; C: grey; H: white. Full colour is available in the electronic version of this paper.

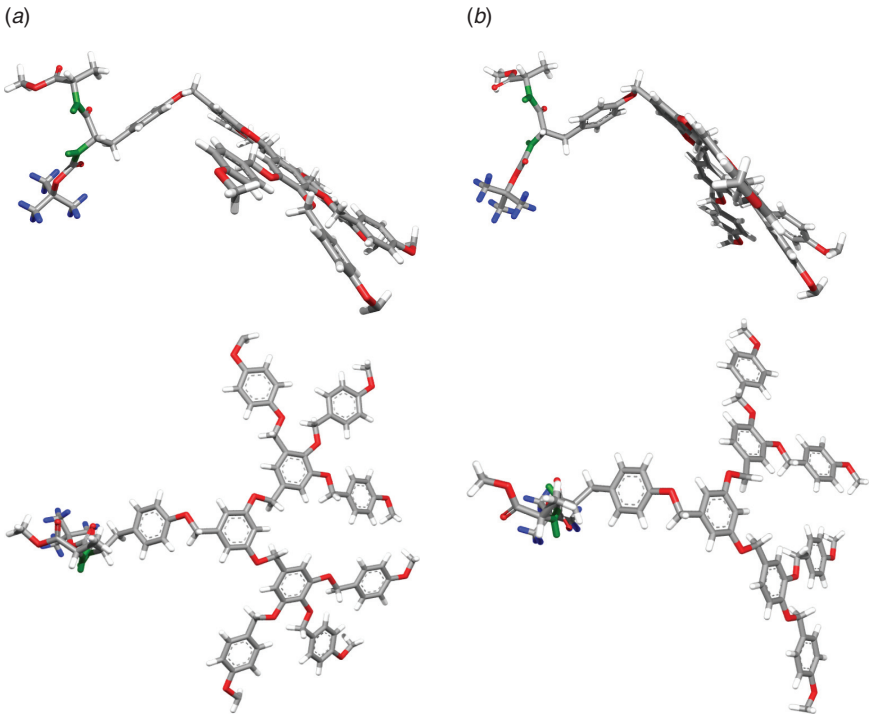

Fig. 7. Side and top views of the dendritic dipeptides (alkyl groups from the periphery are not shown). (*a*) (4-3,4,5-3,5)*n*G$_2$-CH$_2$-Boc-L-Tyr-L-Ala-OMe (*n* = 12, 16); (*b*) (4-3,4-3,5)12G$_2$-CH$_2$-Boc-L-Tyr-L-Ala-OMe.

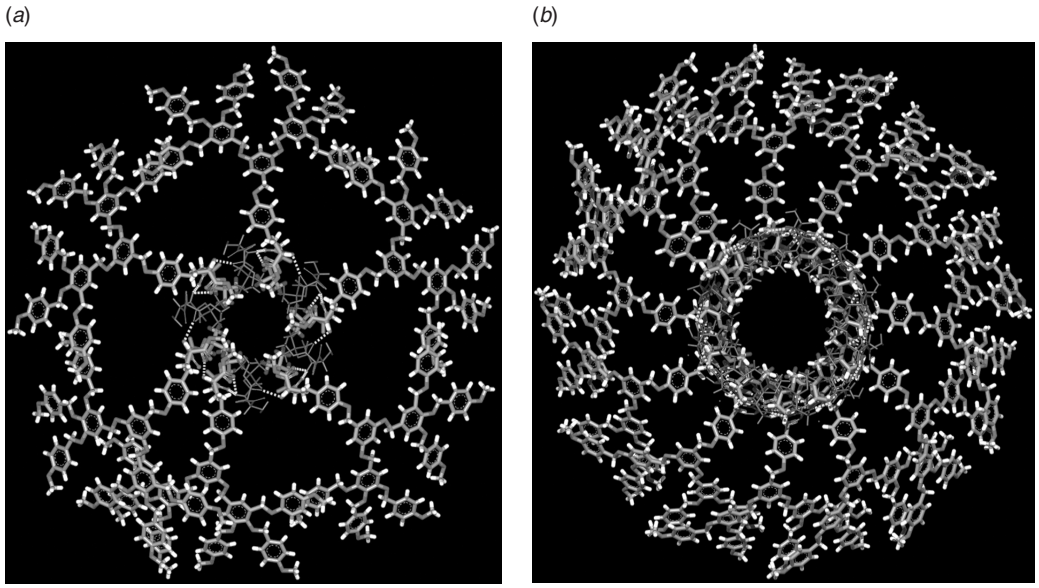

Fig. 8. Single layer top views for the supramolecular columns self-assembled from (*a*) (4-3,4,5-3,5)*n*G_2-CH_2-Boc-L-Tyr-L-Ala-OMe ($n = 12$, 16) and (*b*) (4-3,4-3,5)12G_2-CH_2-Boc-L-Tyr-L-Ala-OMe. Dotted yellow lines indicate the hydrogen-bonding formation. The dipeptides from the next layer are shown in dark grey. Full colour is available in the electronic version of this paper.

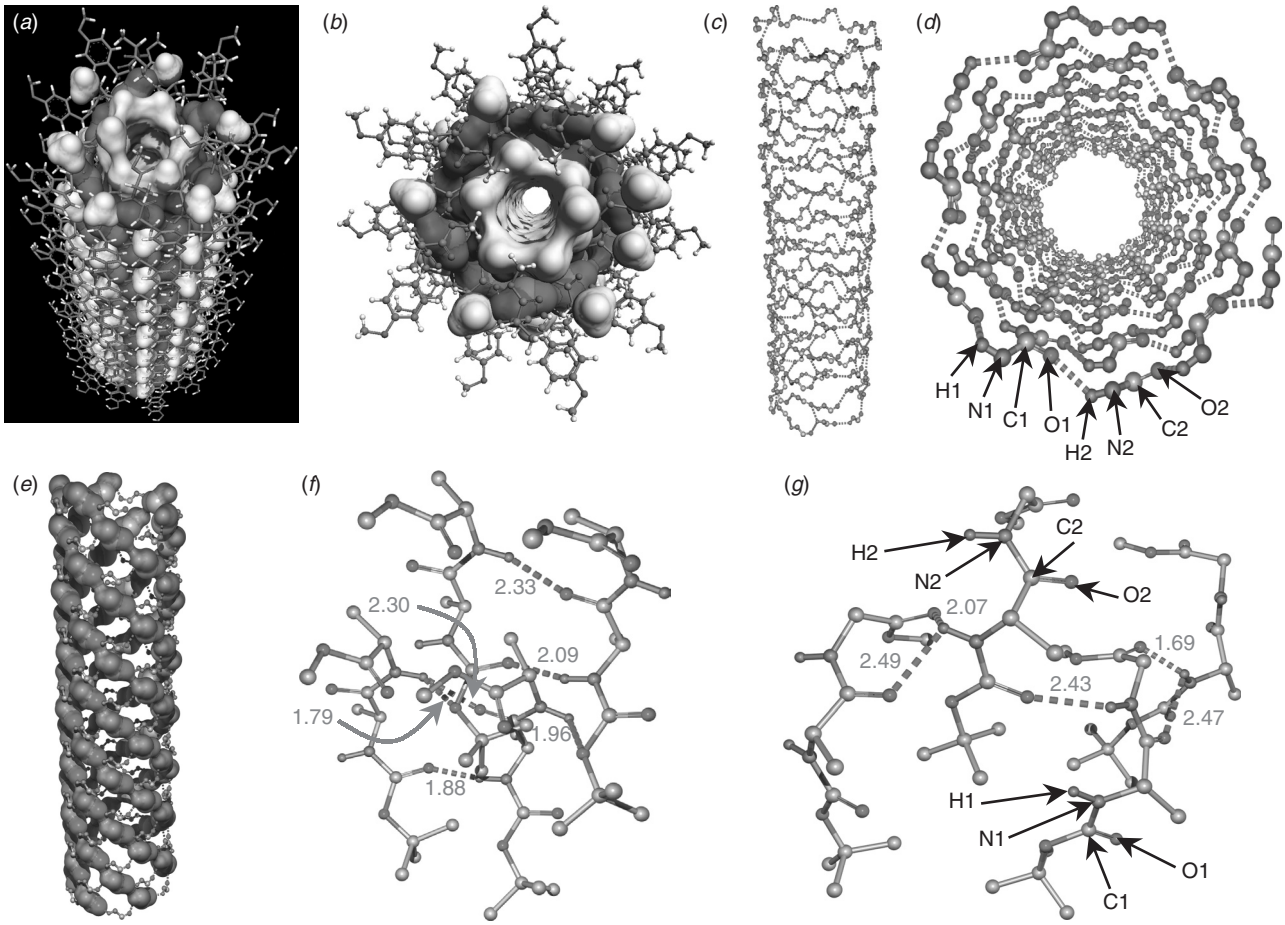

Fig. 9. Supramolecular pore structure detail for (4-3,4,5-3,5)*n*G_2-CH_2-Boc-L-Tyr-L-Ala-OMe ($n = 12$, 16)—(*a*) side and (*b*) top views of the pore region along for a 14-layer molecular model (structure shown up to the phenyl group of Tyr). Hydrogen-bonding network—(*c*) side, (*d*) top, and (*e*) side views, only the H1–N1–C1–O1 and H2–N2–C2–O2 atoms (H green, N green, C grey, O red) of the dipeptide are shown. Hydrogen-bonding detail—(*f*) for (4-3,4-3,5)12G_2-CH_2-Boc-L-Tyr-L-Ala-OMe and (*g*) for (4-3,4,5-3,5)*n*G_2-CH_2-Boc-L-Tyr-L-Ala-OMe ($n = 12$, 16); only the H atoms that participate to hydrogen bonds are shown, indicated bond lengths are in Ångström units. Full colour is available in the electronic version of this paper.

Experimental

Materials

Methyl 4-hydroxybenzoate (99%), 1-bromohexadecane (98%), and allyl bromide (98%) were obtained from Lancaster Synthesis; thionyl chloride (99.5%), $LiAlH_4$ (95%), and anhydrous K_2CO_3 were obtained from Aldrich; methyl 3,4,5-trihydroxybenzoate (97%), 3,5-dihydroxybenzoic acid (97%), palladium(II) acetate (47.5% Pd), cyanuric chloride (99%), 1-bromododecane (98%), and triphenylphosphine (99%) were obtained from Acros Organics; and Boc-L-Tyr-OH (99%), Boc-L-Tyr(OH)-OH (99%), and H_2N-L-Ala-OMe·HCl (99%) were obtained from Bachem Peptides. 2,6-Di-*tert*-butyl-4-methylpyridine (DTBMP) was prepared using a literature procedure.[21] 2-Chloro-4,6-dimethoxy-1,3,5-triazene (CDMT) was obtained from cyanuric chloride following a literature synthesis.[22] Acetone, *N*,*N*-dimethylformamide (DMF), ethyl acetate, magnesium sulfate, and methanol (Fisher ACS reagents) and silica gel (Sorbent Technology) were used as received. THF and dichloromethane (Fisher ACS reagents) were refluxed over sodium/benzophenone and CaH_2, respectively, and freshly distilled before use. Cyclohexane for CD experiments, dichloromethane for HPLC assays, and THF for MALDI-TOF assignments were obtained from Fisher (HPLC grade). Deuterated chloroform for NMR spectra was from Cambridge Isotope Laboratories. All other chemicals were commercially available and were used as received.

Techniques

The purity of the products was determined by a combination of TLC, HPLC, ^{1}H and ^{13}C NMR, MALDI-TOF mass spectrometry, and elemental analysis. TLC was carried on silica gel coated aluminum plates (indicator F_{254}, layer thickness 200 μm, particle size 2–25 μm, pore size 60 Å, Sigma-Aldrich). HPLC was performed in dichloromethane on a high-pressure liquid chromatograph (Series 10, Perkin–Elmer) equipped with a LC-100 column oven, integrator data station (900, Nelson Analytical), and two gel columns of 5×10^2 and 10^4 Å pore size (PL, Perkin–Elmer), using for detection the UV absorbance at 254 nm. ^{1}H (500 MHz) and ^{13}C (125 MHz) NMR spectra were recorded on a DRX 500 instrument (Bruker).

Thermal transitions were measured on a modulated differential scanning calorimeter (DSCQ100, TA Instruments). In all cases the heating and the cooling rates were 10°C min^{-1}. The transition temperatures were measured as the maxima and minima of their endothermic and exothermic peaks. Indium was used as calibration standard. A thermal optical polarized microscope (BX51, 100× magnification, Olympus) equipped with a hot stage (FP82HT, Mettler) and a central processor (FP90, Mettler Toledo) were used to verify thermal transitions and to characterize anisotropic textures. Small parts of the aligned samples were heated on the hot stage up to temperatures close, but always bellow isotropic transition to avoid losing the sample alignment. After a short annealing, image acquisitions were performed. Density measurements were carried out by floatation in gradient columns at 20°C.

MALDI-TOF mass spectrometry was carried out on a mass spectrometer (Voyager-DE, PerSeptive Biosystems) operating in linear mode. The spectrometer equipped with a nitrogen laser (337 nm) was calibrated using the peptides angiotensin II and bombesin as standards. The laser steps and voltages applied were adjusted depending on both the molecular weight and the nature of each analyzed compound. Either 2,5-dihydroxybenzoic acid or 4-hydroxybenzylidenemalononitrile was used as matrix. THF was used for dissolving both matrix and sample (working concentrations: 10 mg mL^{-1} for the matrix and 5–10 mg mL^{-1} for the sample). The analytical sample was obtained by mixing sample and matrix solutions in a 1:5 v/v ratio; 0.5 μL of this resulting solution was loaded onto the MALDI plate and allowed to dry at 23°C before performing the analysis.

Circular dichroism (CD) spectra were recorded on a spectrophotometer (J-720, Jasco) equipped with a variable temperature circulator (RTE-111, NESLAB). Each sample was dissolved in cyclohexane (0.5×10^{-4} M) at 23°C, then heated to 60°C and allowed to cool at 23°C when the solution remained homogenous. CD measurements were performed using a 1-mL quartz cuvette of 0.1 cm path length and the following parameters: scanned optical range 210–320 nm, scan band width 1 nm, scanning speed 100 nm min^{-1}, response 1 s, accumulations 5, scanned thermal ranges 8–60°C, 60–8°C, and 8–60°C, respectively (data pitch 2°C, temperature slope 1°C min^{-1}). Before starting the experiment the sample was allowed to reach the 8°C starting temperature (∼10–15 min) but once started the three thermal cycles were performed successively. Data were processed using *Spectra Manager* ver. 1.51 software (Jasco).

X-ray diffraction measurements were performed using $Cu_{K\alpha 1}$ radiation (λ 1.54178 Å) from a rotating anode X-ray source (FR-591, Bruker–Nonius) with a 0.2×0.2 mm^2 filament operated at 3.4 kW. The beam was collimated and focussed by a single bent mirror and sagitally focussing Ge(111) monochromator, resulting in a 0.3×0.4 mm^2 spot on a multiwire area detector (Hi-Star, Bruker-AXS) 125 cm from the sample. To minimize attenuation and background scattering, an integral vacuum was maintained along the length of the flight tube and within the sample chamber. Powder or aligned samples were held in quartz capillaries (0.7–1.0 mm diameter), then mounted in a temperature controlled oven (temperature precision ±0.1°C, temperature range −120 to 270°C). Sample to multiwire area detector distances are 11.0 cm for wide-angle diffraction experiments and 54.6 cm for intermediate angle diffraction experiments. Aligned samples for fibre XRD experiments were prepared using a custom-made extrusion device. The powdered sample (∼10 mg) was heated inside the extrusion device to isotropic transition temperature. After cooling slowly from the isotropic state, the fibre was extruded in the mesophase and cooled to 23°C. Typically the aligned samples have a thickness of ∼0.3–0.7 mm and a length of ∼3–7 mm. All X-ray diffraction measurements were done with the aligned sample axis perpendicular to the beam direction. X-ray diffraction peaks position and intensity analysis was performed using *Datasqueeze* ver. 20.1 software, that allows background elimination and Gaussian, Lorentzian, Lorentzian-squared, or Voigt peak-shape fitting.

Molecular modelling simulations were performed using the *Materials Studio Modelling* ver. 3.1 software (Accelrys). The package's *Discover* module was used to perform the energy minimizations on the supramolecular structures with the following settings: PCFF or COMPASS force fields, and Flechter–Reeves algorithm for the conjugate gradient method.

*Synthesis of Dendritic Dipeptides (4-3,4,5-3,5)*n*G$_2$-CH$_2$-Boc-L-Tyr-L-Ala-OMe (*n = *12, 16)*

Compounds **2** and **5**,[23] **3** and **6**,[24] and **11**[1] were synthesized according to the procedures published from our laboratory.

*[4-3,4,5]*n*G$_1$CH$_2$OH*

To a 0°C slurry of LAH (1.1 equiv.) in dry THF was added slowly [4-3,4,5]*n*G$_1$CO$_2$CH$_3$ (1 equiv.) in dry THF. Upon addition, the mixture was allowed to stir at 23°C for 1 h, or until TLC (7:1 hexane/EtOAc) showed completion. The reaction mixture was cooled to 0°C and quenched by slow successive addition of H_2O (*x* mL per *x* g of LAH), 15% NaOH (*x* mL per *x* g of LAH), and H_2O (3*x* mL per *x* g of LAH), and stirring continued until H_2 evolution ceased. The reaction mixture was then filtered and the lithium salts were rinsed generously with CH_2Cl_2. The filtrate was dried over $MgSO_4$ and concentrated to give the benzyl alcohol, which was taken to the next step without further purification.

[4-3,4,5]12G$_1$-CH$_2$OH

White solid, 2.35 g (98%), mp 82–83°C. δ_H (500 MHz, $CDCl_3$) 7.32 (d, 4H, *J* 8.8), 7.27 (d, 2H, *J* 8.6), 6.89 (d, 4H, *J* 8.6), 6.76 (d, 2H, *J* 8.6 Hz), 6.65 (s, 2H), 5.01 (s, 4H), 4.93 (s, 2H), 4.57 (s, 2H), 3.94 (m, 6H), 1.78 (m, 6H), 1.45 (m, 6H), 1.39–1.21 (m, 48H), 0.88 (t, 9H, *J* 6.8 Hz). δ_C (125 MHz, $CDCl_3$) 158.9, 153.0, 130.2, 129.1, 114.4, 114.1, 106.6, 74.8, 71.0, 68.0, 67.9, 65.4, 31.9, 29.7, 29.6, 29.4, 29.3 (×2), 26.1, 22.7, 14.1. Found: C 78.4, H 10.1. Calc. for $C_{64}H_{98}O_7$: C 78.5, H 10.1%.

[4-3,4,5]16G$_1$-CH$_2$OH

White solid, 1.02 g (99%), mp 80°C. δ_H (500 MHz, $CDCl_3$) 7.31 (d, 4H, *J* 9.0 Hz), 7.27 (d, 2H, *J* 9.0 Hz), 6.87 (d, 4H, *J* 9.0), 6.75 (d, 2H, *J* 9.0), 6.64 (s, 2H), 5.00 (s, 4H), 4.93 (s, 2H), 4.55 (d, 2H, *J* 5.5), 3.95 (t, 4H, *J* 6.5), 3.91 (t, 2H, *J* 6.5), 1.81–1.71 (m, 6H), 1.48–1.41 (m, 6H), 1.39–1.22 (m, 72H), 0.88 (t, 9H, *J* 7.0). δ_C (125 MHz, $CDCl_3$) 158.9, 153.0, 137.8, 136.4, 130.2, 129.9, 114.4, 114.1, 106.6, 74.8, 71.0, 68.0, 67.9, 65.4, 31.9, 29.7, 29.6 (×2), 29.4, 29.3 (×2), 26.1, 22.7, 14.1. Found: C 79.5, H 10.7. Calc. for $C_{76}H_{122}O_7$: C 79.5, H 10.7%.

*[4-3,4,5]*n*G$_1$-CH$_2$Cl (*n* = 12, 16)*

To a solution of [4-3,4,5]*n*G$_1$-CH$_2$OH (*n* = 12, 16) (1 equiv.) and DTBMP (1.5 equiv.) in dry CH_2Cl_2 was added slowly $SOCl_2$ (1.1 equiv.) and the reaction allowed to stir at 23°C for 5 min. TLC analysis (7:1 Hex:EtOAc) showed completion. Solvent was removed under reduced pressure and the residue was recrystallized from acetone to give the benzyl chlorides **7** and **8**, which decomposed upon melting.

[4-3,4,5]12G$_1$-CH$_2$Cl 7

Off-white solid, 3.77 g (95%). δ_H (500 MHz, $CDCl_3$) 7.33 (d, 4H, *J* 8.8), 7.28 (d, 2H, *J* 8.3), 6.90 (d, 4H, *J* 8.6), 6.77 (d, 2H, *J* 8.6), 6.68 (s, 2H), 3.97 (t, 4H, *J* 6.6), 3.93 (t, 2H, *J* 6.6), 1.79 (m, 6H), 1.46 (m, 6H), 1.40–1.21 (m, 48H), 0.89 (t, 9H, *J* 6.8). δ_C (125 MHz, $CDCl_3$) 158.9, 153.0, 138.6, 132.6, 130.2, 129.7, 129.2, 128.8, 114.4, 114.1, 108.4, 74.8, 71.1, 68.0 (×2), 46.8, 31.9, 29.7, 29.6 (×2), 29.4, 29.3 (×2), 26.1, 22.7, 14.1. Found: C 77.0, H 9.8. Calc. for $C_{64}H_{97}ClO_6$: C 77.0, H 9.8%.

*[4-3,4,5]16G$_1$-CH$_2$Cl **8***

Off-white solid, 2.59 g (89%). δ_H (500 MHz, $CDCl_3$) 7.31 (d, 4H, *J* 8.5), 7.26 (d, 2H, *J* 8.5), 6.88 (d, 4H, *J* 8.5), 6.75 (d, 2H, *J* 8.5), 6.67 (s, 2H), 5.01 (s, 4H), 4.93 (s, 2H), 4.48 (s, 2H), 3.96 (t, 4H, *J* 6.5), 3.92 (t, 2H, *J* 6.5), 1.80–1.71 (m, 6H), 1.48–1.40 (m, 6H), 1.38–1.20 (m, 72H), 0.88 (t, 9H, *J* 7.0). δ_C (125 MHz, $CDCl_3$) 158.9, 153.0, 137.8, 130.2, 129.9, 114.4, 114.1, 106.6, 74.8, 71.0, 68.0, 67.9, 65.4, 31.9, 29.7, 29.6 (×2), 29.4, 29.3 (×2), 26.1, 22.7, 14.1. Found: C 78.3, H 10.4. Calc. for $C_{76}H_{121}ClO_6$: C 78.3, H 10.5%.

*3,5-Diallyloxybenzyl Chloride **10***

A mixture of methyl 3,5-dihydroxybenzoate (1.00 g, 5.95 mmol), K_2CO_3 (2.46 g, 17.8 mmol) and allyl bromide (1.44 g, 11.9 mmol) in acetone (80 mL) was refluxed under argon for 4 h. TLC analysis (5% MeOH in CH_2Cl_2) showed completion of reaction. After cooling to 23°C, the reaction mixture was partitioned between ethyl acetate and water. The organic phase was washed with water (3×), dried over $MgSO_4$, and concentrated under reduced pressure. The crude product was passed through a silica plug eluted with 7:1 hexane/EtOAc to give the methyl 3,5-diallyloxybenzoate as a clear oil which was taken up in dry THF (15 mL) and added slowly to a suspension of LAH (250 mg, 6.55 mmol) in dry THF (10 mL). After stirring for 30 min at 23°C, TLC analysis (7:1 hexane/EtOAc) showed completion. Reaction was quenched by slow successive addition of water (250 μL), followed by 15% aqueous NaOH (250 μL), and water (750 μL). Stirring was continued until H_2 evolution ceased, and the resulting lithium salts were filtered off and rinsed generously with CH_2Cl_2, the filtrate was dried over $MgSO_4$, and concentrated under reduced pressure to give 1.20 g (92% over two steps) of the diallyloxybenzyl alcohol. This diallyloxybenzyl alcohol (1.20 g, 5.45 mmol) was taken up in dry CH_2Cl_2 (40 mL) and a catalytic amount of DMF added. To this solution was slowly added $SOCl_2$ (707 mg, 5.99 mmol), and the reaction was stirred at 23°C for 5 min after which TLC analysis (7:1 hexane/EtOAc) showed completion. The reaction mixture was diluted with CH_2Cl_2 and quenched by slow addition of water. The phases were separated and the organic phase was washed with water (1×) and saturated aqueous $NaHCO_3$ (2×). The organic phase was dried over $MgSO_4$ and concentrated under reduced pressure to give 1.20 g (92%) of 3,5-diallyloxybenzyl chloride **10** as a yellow oil, which was used without further purification. δ_H (500 MHz, $CDCl_3$) 6.54 (d, 2H, *J* 2.5), 6.44 (t, 1H, *J* 2), 6.06–5.99 (m, 2H), 5.41 (m, 1H), 5.38 (m, 1H), 5.28 (m, 1H), 5.26 (m, 1H), 4.50 (m, 4H), 4.48 (s, 2H). δ_C (125 MHz, $CDCl_3$) 159.8, 139.4, 132.9, 117.7, 107.4, 101.8, 68.9, 46.2. Found: C 65.4, H 6.3. Calc. for $C_{13}H_{15}ClO_2$: C 65.4, H 6.3%.

*[3,5]AllylG$_1$-CH$_2$-Boc-L-Tyr-L-Ala-OMe **12***

Boc-L-Tyr(OH)-L-Ala-OMe **11** (200 mg, 0.546 mmol) was added to a degassed suspension of K_2CO_3 (226 mg, 1.64 mmol) in DMF (10 mL) and heated to 70°C, then 3,5-diallyloxybenzyl chloride (**11**) (143 mg, 0.600 mmol) was added. The reaction mixture was stirred overnight at 70°C, cooled to 23°C and taken up in EtOAc, washed with water (5×), brine, dried over $MgSO_4$, and concentrated under reduced pressure. The crude product was purified by flash column chromatography: silica gel/2% MeOH in CH_2Cl_2 to give 210.5 mg (68%) of the [3,5]allyl-G$_1$-CH$_2$Boc-L-Tyr-L-Ala-OMe **12** as a yellowish oil. δ_H (500 MHz, $CDCl_3$) 7.10 (d, 2H, *J* 8.5), 6.88 (d, 2H, *J* 8.5), 6.59 (m, 2H), 6.44 (m, 1H), 6.37 (d, 1H, *J* 2.5), 6.07–5.99 (m, 2H), 5.41 (m, 1H), 5.38 (m, 1H), 5.28 (m, 1H), 5.26 (m, 1H), 4.96 (s, 3H), 4.51 (d, 2H, *J* 5.5), 4.29 (s, 1H), 3.71 (s, 3H), 3.07–2.96 (m, 2H), 1.42 (s, 9H), 1.34 (d, 3H, *J* 7.0). δ_C (125 MHz, $CDCl_3$) 172.8, 170.7, 159.9, 139.4, 133.1, 130.4, 117.7, 115.1, 106.1, 101.3, 69.9, 68.9, 52.4, 48.1, 37.4, 28.2, 18.4. Found: C 65.5, H 7.1, N 4.9. Calc. for $C_{31}H_{40}N_2O_8$: C 65.5, H 7.1, N 4.9%.

*[3,5]OHG$_1$-CH$_2$-Boc-L-Tyr-L-Ala-OMe **13***

Palladium(II) acetate (4 mg, 0.018 mmol) was added to a thoroughly degassed solution of [3,5]allylG$_1$-CH$_2$Boc-L-Tyr-L-Ala-OMe **12** (210 mg, 0.369 mmol), PPh_3 (24 mg, 0.092 mmol), and Et_3NHCO_2H (164 mg, 1.11 mmol) in EtOH (20 mL). The reaction mixture was refluxed overnight, cooled to room temperature and then taken up in EtOAc, washed with water (3×), brine, dried over $MgSO_4$, and concentrated under reduced pressure. The crude product was purified by flash column chromatography (silica gel/5% MeOH in CH_2Cl_2) to give 124.5 mg (70%) of [3,5]OHG$_1$-CH$_2$Boc-L-Tyr-L-Ala-OMe **13** as off-white crystals. δ_H (500 MHz, $CDCl_3$) 6.96 (br s, 4H), 6.75 (d, 2H, *J* 9), 6.65 (s, 1H), 6.41 (s, 2H), 6.32 (s, 1H), 5.21 (br s, 1H), 4.84 (s, 2H), 4.48 (m, 1H), 4.27 (br s, 1H), 3.66 (s, 3H), 2.91 (m, 2H), 1.29 (d, 3H, *J* 7.0). δ_C (125 MHz, $CDCl_3$) 172.8, 170.8, 157.9, 137.0, 130.4, 128.5, 127.4, 115.0, 70.0, 52.3, 48.0, 37.4, 33.9, 28.2, 18.3. Found: C 61.5, H 6.6, N 5.7. Calc. for $C_{25}H_{32}N_2O_8$: C 61.5, H 6.6, N 5.7%.

*[4-3,4,5-3,5]*n*G$_2$-CH$_2$-Boc-L-Tyr-L-Ala-OMe (*n* = 12, 16)*

[3,5]OHG$_1$-CH$_2$-Boc-L-Tyr-L-Ala-OMe **13** (1 equiv.) was added to a thoroughly degassed suspension of K_2CO_3 (3 equiv.) in DMF. The resulting mixture was heated to 70°C, at which point the tri-substituted benzyl chloride **7** or **8** (2 equiv.) was added. The reaction was stirred at 70°C overnight, cooled to 23°C and the product was precipitated into water, collected by suction filtration, air dried, and purified by flash column chromatography (silica gel/1% MeOH in CH_2Cl_2) followed by precipitation in MeOH from minimal CH_2Cl_2 to give dendritic dipeptides **14** or **15** as off-white solid.

*[4-3,4,5-3,5]12G$_2$-CH$_2$-Boc-L-Tyr-L-Ala-OMe **14***

Off-white solid, 120 mg (61%). mp 96–98°C, $[\alpha]_D^{20}$ −8.3 (*c* 0.05 in THF). *m/z* (MALDI-TOF) for $C_{153}H_{224}N_2O_{20}$ calc. 2434.41 [M + Na^+]; found 2434.43. HPLC > 99% pure. δ_H (500 MHz, $CDCl_3$) 7.30 (d, 8H, *J* 8.5), 7.27 (d, 4H, *J* 8.5), 7.11 (d, 2H, *J* 8.5), 6.90 (d, 2H, *J* 8.5), 6.86 (d, 8H, *J* 8.5), 6.75 (d, 4H, *J* 8.5), 6.73 (s, 4H), 6.68 (m, 2H), 6.56 (m, 1H), 6.34 (d, 1H, *J* 7.0), 5.00 (s, 8H), 4.97 (s, 2H), 4.91 (d, 8H, *J* 3.5), 4.51 (m, 1H), 4.25 (br s, 1H), 3.96–3.90 (m, 12H), 3.69 (s, 3H), 3.05–2.94 (m, 2H), 1.80–1.72 (m, 12H), 1.45 (m, 12H), 1.41 (s, 9H), 1.34 (d, 3H, *J* 7.0), 1.33–1.20 (m, 96H), 0.88 (t, 18H, *J* 6.5). δ_C (125 MHz, $CDCl_3$) 170.7, 160.2, 159.0 (×2), 149.4, 149.1, 139.4, 130.4 (×2), 130.1, 129.2, 129.1, 129.0, 121.0, 115.5, 115.1, 114.5, 106.4, 101.5, 71.4, 71.3, 70.1, 70.0, 68.1, 52.4, 48.1, 31.9, 29.7, 29.6, 29.4, 29.3, 28.3, 26.1, 22.7, 18.4, 14.1. Found: C 76.2, H 9.3, N 1.2%. Calc. for $C_{153}H_{224}N_2O_{20}$: C 76.2, H 9.4, N 1.2%.

[4-3,4,5-3,5]16G$_2$-CH$_2$-Boc-L-Tyr-L-Ala-OMe ***15***

Off-white solid, 105 mg (60%). mp 119–120°C, $[\alpha]_D^{20}$ −7.9 (*c* 0.05 in THF). *m/z* (MALDI-TOF) for $C_{177}H_{272}N_2O_{20}$ calc. 2771.05 $[M + Na^+]$; found 2771.04. HPLC > 99% pure. δ_H (500 MHz, $CDCl_3$) 7.31 (d, 8H, *J* 8.0), 7.26 (d, 4H, *J* 8.0), 7.10 (d, 2H, *J* 8.0), 6.91 (d, 2H, *J* 8.0), 6.86 (d, 8H, *J* 8.0), 6.77 (d, 4H, *J* 8.0), 6.73 (s, 4H), 6.68 (m, 2H), 6.55 (m, 1H), 6.35 (d, 1H, *J* 7.0), 5.00 (s, 8H), 4.97 (s, 2H), 4.91 (d, 8H, *J* 3.5), 4.51 (m, 1H), 4.25 (br s, 1H), 3.96–3.90 (m, 12H), 3.69 (s, 3H), 3.06–2.94 (m, 2H), 1.80–1.72 (m, 12H), 1.45 (m, 12H), 1.41 (s, 9H), 1.34 (d, 3H, *J* 7.0), 1.32–1.20 (m, 144H), 0.88 (t, 18H, *J* 7.0). δ_C (125 MHz, $CDCl_3$) 170.7, 160.2, 159.0 (×2), 149.4, 149.1, 139.4, 130.4 (×2), 130.1, 129.2, 129.1 (×2), 129.0, 121.0, 115.6, 115.1, 114.5, 106.4, 101.5, 71.4 (×2), 70.1, 70.0, 68.1, 52.4, 48.1, 31.9, 29.7, 29.6 (×2), 29.4, 29.3 (×2), 28.3, 26.1, 22.7, 18.4, 14.1. Found: C 77.38, H 10.0, N 1.0. Calc. for $C_{177}H_{272}N_2O_{20}$: C 77.4, H 10.0, N 1.0%.

Acknowledgments

Financial support by the National Science Foundation (DMR-9996288 and DMR-0102459) and the Office of Naval Research is gratefully acknowledged.

References

[1] V. Percec, A. E. Dulcey, V. S. K. Balagurusamy, Y. Miura, J. Smidrkal, M. Peterca, S. Nummelin, U. Edlund, S. D. Hudson, P. A. Heiney, H. Duan, S. N. Maganov, S. A. Vinogradov, *Nature* **2004**, *430*, 764. doi:10.1038/NATURE02770

[2] A. Klug, *Angew. Chem. Int. Ed. Engl.* **1983**, *22*, 565. doi:10.1002/ANIE.198305653

[3] R. MacKinnon, *Angew. Chem. Int. Ed.* **2004**, *43*, 4265. doi:10.1002/ANIE.200400662

[4] P. Agre, *Angew. Chem. Int. Ed.* **2004**, *43*, 4278. doi:10.1002/ANIE.200460804

[5] K. Braig, Z. Otwinowski, R. Hegde, D. C. Boisvert, A. Joachimiak, A. L. Horwich, P. B. Sigler, *Nature* **1994**, *371*, 578. doi:10.1038/371578A0

[6] D. Ishii, K. Kinbara, Y. Ishida, N. Ishii, M. Okochi, M. Yohda, T. Aida, *Nature* **2003**, *423*, 628. doi:10.1038/NATURE01663

[7] H. Bayley, P. S. Cremer, *Nature* **2001**, *413*, 226. doi:10.1038/35093038

[8] E. Gouaux, *J. Struct. Biol.* **1998**, *121*, 110. doi:10.1006/JSBI.1998.3959

[9] S. Fernandez-Lopez, H.-S. Kim, E. C. Choi, M. Delgado, J. R. Granja, A. Khasanov, K. Kraehenbuehl, G. Long, D. A. Weinberger, K. M. Wilcoxen, M. R. Ghadiri, *Nature* **2001**, *412*, 452. doi:10.1038/35086601

[10] V. Percec, W.-D. Cho, G. Ungar, D. J. P. Yeardley, *J. Am. Chem. Soc.* **1998**, *120*, 4417. doi:10.1021/JA9735315

[11] M. R. Ghadiri, R. J. Granja, R. A. Milligan, D. E. McRee, N. Khazanovich, *Nature* **1993**, *366*, 324. doi:10.1038/366324A0

[12] H. Fenniri, B.-L. Deng, A. E. Ribbe, *J. Am. Chem. Soc.* **2002**, *124*, 11064. doi:10.1021/JA026164S

[13] S. Hecht, *Mater. Today* **2005**, *8*, 48. doi:10.1016/S1369-7021(05)00747-9

[14] S. D. Hudson, H.-T. Jung, V. Percec, W.-D. Cho, G. Johansson, G. Ungar, V. S. K. Balagurusamy, *Science* **1997**, *278*, 449. doi:10.1126/SCIENCE.278.5337.449

[15] V. Percec, C.-H. Ahn, G. Ungar, D. J. P. Yeardley, M. Möller, S. S. Sheiko, *Nature* **1998**, *391*, 161. doi:10.1038/34384

[16] V. Percec, M. Glodde, T. K. Bera, Y. Miura, I. Shiyanovskaya, K. D. Singer, V. S. K. Balagurusamy, P. A. Heiney, I. Schnell, A. Rapp, H.-W. Spiess, S. D. Hudson, H. Duan, *Nature* **2002**, *419*, 384. doi:10.1038/NATURE01072

[17] G. Ungar, Y. Liu, X. Zeng, V. Percec, W.-D. Cho, *Science* **2003**, *299*, 1208. doi:10.1126/SCIENCE.1078849

[18] X. Zeng, G. Ungar, Y. Liu, V. Percec, A. Dulcey, J. K. Hobbs, *Nature* **2004**, *428*, 157. doi:10.1038/NATURE02368

[19] J. J. L. M. Cornelissen, A. E. Rowan, R. J. M. Nolte, N. A. J. M. Sommerdijk, *Chem. Rev.* **2001**, *101*, 4039. doi:10.1021/CR990126I

[20] L. Brunsveld, B. J. B. Folmer, E. W. Meijer, R. P. Sijbesma, *Chem. Rev.* **2001**, *101*, 4071. doi:10.1021/CR990125Q

[21] P. J. Stang, A. G. Anderson, *J. Org. Chem.* **1976**, *41*, 3034. doi:10.1021/JO00867A007

[22] J. S. Kronin, F. O. Ginah, A. R. Murray, J. D. Copp, *Synth. Commun.* **1996**, *26*, 3491.

[23] V. Percec, C. M. Mitchell, W.-D. Cho, S. Uchida, M. Glodde, G. Ungar, X. Zeng, Y. Liu, V. S. K. Balagurusamy, P. A. Heiney, *J. Am. Chem. Soc.* **2004**, *126*, 6078. doi:10.1021/JA049846J

[24] V. Percec, C.-H. Ahn, W.-D. Cho, A. M. Jamieson, J. Kim, T. Leman, M. Schmidt, M. Gerle, M. Möller, S. A. Prokhorova, S. S. Sheiko, S. Z. D. Cheng, A. Zhang, G. Ungar, D. J. P. Yeardley, *J. Am. Chem. Soc.* **1998**, *120*, 8619. doi:10.1021/JA981211V